IONIC CONTACTS AT DnaK SUBSTRATE BINDING DOMAIN INVOLVED IN THE ALLOSTERIC REGULATION OF LID DYNAMICS

Vanesa Fernández-Sáiz[1,2], Fernando Moro[1,2], Jesus M. Arizmendi[2], Sergio P. Acebrón[1,2] and Arturo Muga[1,2]*

[1]Unidad de Biofísica (CSIC-UPV/EHU) and [2]Departamento de Bioquímica y Biología Molecular, Facultad de Ciencias, Universidad del País Vasco. Aptdo. 644, 48080 Bilbao, Spain.

Running title: Allosteric communication in DnaK

*corresponding author: Arturo Muga: Tel.: +34 946012624; Fax: +34 944648500; E-mail: gbpmuvia@lg.ehu.es

To gain further insight into the interactions involved in the allosteric transition of DnaK we have characterized wt protein and three mutants in which ionic interactions at the interface between both subdomains and within the lid subdomain have been disrupted. Our data show that ionic contacts, most likely forming an electrically charged network, between the N-terminal region of helix B and an inner loop of the β-sandwich are involved in maintaining the position of the lid relative to the β-subdomain in the ADP- but not in the ATP-state of the protein. Disruption of the ionic interactions between the C-terminal region of helix B and the outer loops of the β-sandwich, known as the latch, does not have the same conformational consequences, but results equally in an inactive protein. This points to a variety of mechanisms that can inactivate this complex allosteric machine. Our results identify the ionic contacts at the subdomain and interdomain interfaces that are part of the hinge region involved in the ATP-induced allosteric displacement of the lid away from the peptide binding site. These interactions also stabilize peptide-Hsp70 complexes at physiological (37ºC) and stress (42ºC) temperatures, a requirement for productive substrate (re)folding.

The ubiquitous Hsp70 chaperone proteins are essential to prevent aggregation of misfolded proteins under heat shock conditions. They also participate in cellular processes such as folding of newly synthesized polypeptides, protein translocation across membranes, assembly and disassembly of protein complexes and refolding of protein aggregates (1).

Hsp70 proteins consist of two major structural domains: a conserved N-terminal ATPase domain and a more variable C-terminal substrate binding domain (SBD). The SBD contains a β-sandwich, that holds the peptide binding groove, and an α-helical subdomain that folds over the β-structure and might control accessibility of the peptide binding site. High resolution three dimensional structures of isolated forms of both structural domains with different bound ligands have been reported (2-11). Recently a model of a two-domain truncated Hsp70 from *Thermus thermophilus* has been proposed based on NMR studies (12). Some of the interdomain contacts are better revealed in the X-ray structure of a bovine Hsc70 that lacks most of the SBD helical subdomain (13). In DnaK, the best known bacterial representative of the Hsp70 family, the substrate peptide is bound in an extended conformation between two loops that protrude from the β-sandwich subdomain ($L_{1,2}$ and $L_{3,4}$), and are in turn buttressed by two other loops ($L_{4,5}$ and $L_{5,6}$). The helical subdomain of the SBD acts like a lid over the β-sandwich subdomain. The α-helices A and B are packed onto the β-sandwich and helix B covers the substrate binding cavity. The distal part of helix B, together with helices C, D and E, builds up a hydrophobic helical core that acts as a "lid" (6,9). Although interdomain coupling occurs in the absence of the lid and the bound peptide contacts the β-structure but not the α-helical subdomain, its presence has confirmed to be essential in stabilizing Hsp70-substrate complexes (14,15), especially at stress temperatures (16).

The broad spectrum of activities that Hsp70 proteins exhibit requires their interaction with hydrophobic segments of (partially) unfolded polypeptide chains, in a nucleotide-

controlled unknown mechanism (17). When ATP binds the ATPase domain of Hsp70s an allosteric signal is transmitted to the SBD that adopts a conformation with fast substrate association and dissociation rates, and therefore low substrate affinity. In contrast, the substrate is tightly bound to the ADP-bound conformation which displays a high affinity for substrates (18).

One of the most important characteristics of DnaK conformations, that has been proposed to dictate their affinity for peptides, is the position of the lid relative to the β-subdomain of the SBD. The displacement of the lid away from the peptide binding site seems to facilitate substrate dissociation (18). Therefore, analysis of the interactions that anchor the lid to the β-subdomain at the SBD might be relevant to localize the hinge regions of the protein that allow lid movement. Among these interactions, those in which helix B is involved seem to be especially relevant, since residues at this helical segment interact with amino acids belonging to both SBD folding units (6). In this work, we systematically compare three mutants of DnaK that lack different ionic interactions between residues at helix B and amino acids at the lid and β-subdomains, respectively. Our results indicate that the salt bridge D526-R445 plays a pivotal role in properly positioning the lid, relative to the β-subdomain. Data presented here favor a structural transition between the open and closed DnaK conformations that involves structural changes in the α-helical subdomain larger than those initially proposed from the DnaK SBD crystal structure (6).

Experimental Procedures

Site-directed Mutagenesis of DnaK and purification of proteins − Mutants DnaK1A, DnaK2A and DnaK3A were obtained by sequential PCR steps using DnaK flanking primers (19) and mutagenic primers (underlined letters show the nucleotides changed for each mutation): *A* 5´-GVVGAAGCTGCCCGTAAGTTG-3´ and *B* 5´-CTTACGGGCAGCTTCGGCG-3´,for DnaK1A (D526A); *C* 5´-CGCCCATCTGCTGCACAGCACCCGTGCCAGGTTGAAG-3´ and *D* 5´-GCGCACGGGTGCTGTGCAGCAGATGGGCGCCCTGG-3´, for DnaK2A (D540A/K548A); *E* 5-GAAGCGCTGGTACAGACTGCCAACCAGGCG-3´, *F* 5´-GTTGGCAGTCTGTACCAGCGCTTCAAAC-3´, *G* 5´-CACAGCACCGCTAAGCAGGTTGAAGAAG-3´ and *H* 5´-CTGCTTAGCGGTGCTGTGCAG-3´ for DnaK3A (E531A/R536A/R547A). PCR products were cloned into the bacterial expression vector pTrc99A (Amersham, Pharmacia, Biotech.) as described previously (19), and sequenced to verify the encoded proteins. DnaK wild type and mutants were expressed, purified and extensively dialyzed to obtain nucleotide-free samples (20).

DnaJ and GrpE were expressed in BL21 cells and purified as described elsewhere (21,22). Protein concentration was determined by the colorimetric Bradford assay (Bio-Rad, Munich, Germany.)

Peptide binding − F-APPY peptide (fluorescein-CALLQSRLLLSAPRRAAATARY) binding experiments were performed in 25 mM Hepes, pH 7.6, 50 mM KCl, 5 mM $MgCl_2$, 1 mM DTT. To ensure equilibrium, mixtures containing 35 nM F-APPY and different Hsp70 concentrations (from 1 nM to 50 μM) were incubated overnight at 4ºC. Fluorescence anisotropy data were recorded on a SLM8100 spectrofluorimeter (Aminco) with excitation at 492 nm, emission at 516 nm and slit widths of 8 nm. The fraction of peptide bound for each Hsp70 protein concentration was calculated and the data were fitted as described previously (23,24). Peptide binding kinetics were analyzed at 25ºC, 37ºC and 42ºC using F-APPY and Hsp70 concentrations of 35 nM and 1 μM (wt DnaK, DnaK1A and DnaK2A) or 3 μM (DnaK3A) Hsp70, respectively, as well as 0.5 mM ADP to stabilize the ATPase domain at stress temperatures. Data were fitted to a monoexponential equation consistent with a bimolecular reaction and the k_{obs} value was plotted against Hsp70 concentration to obtain the binding parameters k_{+1} and k_{-1} as described (14,24).

Circular dichroism − Far-UV circular dichroism (CD) spectra were recorded in a Jasco J-810 spectropolarimeter equipped with a thermoelectric cell holder. The collection parameters were 0.5 mm pathlength, 1 nm bandwidth, 50 nm min^{-1} scan rate, and 0.5 seconds response time. Scans were performed at 20ºC in 10 mM sodium borate (pH 9.0) and 0.3 $mg \cdot ml^{-1}$ protein concentration. Spectra were averaged from 10 scans and normalized for protein concentration. For the thermal stability experiments, the mean residue ellipticity at 222

nm was monitored using a 2 mm pathlength cell, and temperature was increased from 20ºC to 90ºC at a scanning rate of 60ºC h^{-1} .

Differential scanning calorimetry − DSC was performed in a VP-DSC microcalorimeter (Microcal, Northampton, MA). Protein samples were extensively dialyzed against 25 mM glycine, pH 9.0, centrifuged to remove aggregates and degassed prior to be loaded in the calorimeter. At pH 9.0 the solubility of the thermally denatured conformation is high enough to make the denaturation transition highly reversible (25). Experiments were carried out under positive pressure to avoid degassing during heating. The calorimetric data were analyzed using ORIGIN software provided with the calorimeter. Protein concentration was 1-2 $mg \cdot ml^{-1}$ and the scanning rate was 60 $ºC \cdot h^{-1}$. Experiments were carried out at least twice, on two different batches of each protein.

Partial Proteolysis by trypsin − Partial proteolysis of wild type DnaK and mutants was carried out in 40 mM Hepes buffer, 50 mM KCl, 10 mM $MgCl_2$, pH 7.6. 5 µM Hsp70 proteins were incubated at 30º with 1.6 U of trypsin, in the absence or presence of 1mM ATP or ADP. Aliquots containing 5 µg of protein were taken at different incubation times and diluted directly into Laemmli loading buffer for 12.5% SDS−PAGE analysis.

Mass Spectrometry analysis

− *In gel digestion* − Selected tryptic bands were cut from Coomassie stained, fixed gels and subjected to in gel tryptic digestion according to Shevchenko et al. (26) with minor modifications. The gel pieces were swollen in a digestion buffer containing 50 mM NH_4HCO_3 and 12.5 $ng \cdot \mu l^{-1}$ trypsin (Roche Diagnostics, recombinant, proteomic grade trypsin, Penzberg, Germany) in an ice bath. After 30 min the supernatant was removed and discarded and 20 µl of 50 mM NH_4HCO_3 were added to the gel piece, the digestion proceeding at 37ºC overnight. Supernatant was recovered and peptides were extracted twice: first with 25 mM NH_4HCO_3 and acetonitrile (ACN) (Romil, Cambridge, UK) and second with 0,1% TFA and ACN. Supernatants of each sample were pooled and dried in a speed-vac. Prior to MS analysis, pellets were resuspended in 10 µl of 0.1 % trifluoracetic acid (TFA) (Merck, Darmstadt, Germany) for MALDI-MS and in 10 µl of 0,1 % formic acid (FA) (Merck) for ESI-MS analysis and sonicated for 5 minutes.

− *Sample preparation for MALDI-MS analysis* − Recovered peptides were purified prior to MALDI analysis using home made nano-columns as described by Gobom et al. (27) with some modifications. A column consisting of 100-300 nl of activated charcoal from Sigma (C-5510) was packed in a constricted GELoader tip (Eppendorf, Hamburg, Germany) (28). A 1 ml syringe was used to force liquid through the column by appliying air pressure. The column was equilibrated and washed with 0.1 % TFA, and bound peptides were subsequently eluted directly onto the MALDI target with 0.5 µl CHCA solution (α-cyano-4-hydroxycinnamic acid 20 $\mu g \cdot \mu l^{-1}$ in ACN, TFA, 70:30, v/v).

− *MALDI-MS analysis* − Peptide mass fingerprinting was performed on a Bruker Ultraflex TOF/TOF mass spectrometer (Bruker-Daltonics, Bremen, Germany). Positively charged ions were analyzed in reflector mode, using delayed extraction. The spectra were obtained by randomly scanning the sample surface. Typically 200-300 spectra were averaged to improve the signal to noise ratio. Spectra were externally calibrated resulting in a mass accuracy of <70 ppm. Protein identification was performed by searching in a non-redundant protein database (NCBI) using Mascot searching engine (http://www.matrixscience.com). The following parameters were used for database searches: one missed cleavages was allowed, and carbamidomethylation of cysteine and oxidation of methionine were selected as fixed and variable modification, respectively.

− *ESI-MS analysis* − Tandem electrospray mass spectra were acquired using a Micro Q-TOF (Waters Corporation, Milford, MA, USA) mass spectrometer interfaced to a CapLC capillary chromatograph. 7 µl of sample was loaded onto a Symetry300 C18 NanoEase Trap precolumn (Waters, Mildford, MA, USA) and washed with 0.1% FA for 5 minutes at a flow rate of 20 $\mu L \cdot min^{-1}$. Precolumn was connected to an Atlantis dC18 NanoEase column (Waters) equilibrated in 5% ACN, 0.1% FA. A flow splitter was used to decrease the flow rate to 200 $nl \cdot min^{-1}$ and peptides were eluted with a 30 minutes linear gradient from 10% to 60% ACN directly to the nano-electrospray capillary tip (New Objective, Woburn, MA, USA). The capillary voltage was set to 1750 V and data

dependent MS/MS acquisitions were performed on precursors with charge states of 2, 3 or 4 over a survey *m/z* range of 400-1500. Obtained spectra were searched against the Swiss-Prot database using ProteinLynx Global Server 2.1 (Waters). For protein identification the following parameters were adopted: complete carbamidomethylation of cysteines; 25 ppm peptide mass tolerance; 0.05 Da fragment mass tolerance; and 1 missed cleavages. When the presence of a particular peptide on a sample was checked, an inclusion list of m/z of the precursor was used for the MS/MS acquisition.

Functional assays

− *ATPase activity* − Steady-state ATPase activity was assayed in 40 mM Hepes, pH 7.5, 50 mM KCl, 11 mM Mg-acetate buffer at 30ºC, as described previously (19). Protein and ATP concentration were 3 μM Hsp70 and 1 mM, respectively. Reactions were followed measuring the absorbance decay at 340 nm for 30 min in a Cary spectrophotometer (Varian). In the peptide and cochaperone stimulation assays, NRLLLTG (NR) peptide was added at a final concentration of 100-fold and DnaJ and GrpE were added at 0.3 and 0.9 μM respectively, as previously described (29).

− *Refolding of denatured luciferase* − Luciferase was denatured for 45 min at 25ºC, in 6 M GdnHCl, 100 mM Tris, pH 7.7, 10 mM DTT. Refolding was achieved by diluting luciferase to 25 nM in 50 mM Tris, pH 7.7, 55 mM KCl, 15 mM $MgCl_2$, 5.5 mM DTT, 0.5 $mg \cdot ml^{-1}$ bovine serum albumin, containing an ATP regenerating system (4 mM phosphoenolpyruvate and 20 $ng \cdot ml^{-1}$ pyruvate kinase) and 6 μM Hsp70, 6 μM DnaJ and 7.2 μM GrpE. Reactivation was initiated by addition of 5 mM ATP. Luciferase activity was measured after a 90 min reactivation period at at 25ºC, 37ºC or 42ºC, using the luciferase assay system (Promega E1500) in a Sinergy HT (Biotek) luminometer.

RESULTS

Design of mutants

Analysis of the ionic interactions at the SBD reveals that in six of the ionic contacts found, one of the involved residues is located in helix B. This helical segment communicates the helical and β-subdomains participating, *via* its N-terminal region, in the folding unit formed by the β-sandwich and helix A, and through its C-terminal region, in the second folding unit formed by the remaining helical segments of the lid subdomain (6). To analyze the effect of these ionic contacts in the structural and functional properties of DnaK, each corresponding residue in helix B was substituted by alanine (Fig. 1A). It is important to note that none of the mutated residues were located in the β-sandwich subdomain, since this might modify the peptide substrate binding properties of the protein. In the first mutant -DnaK(D526A)-, named DnaK1A, a salt bridge between the N-terminal half of helix B and the inner loops of the β-sandwich subdomain is disrupted. The second mutant, DnaK2A, bears two mutations (D540A/K548A) that break a salt bridge and a hydrogen bond between the C-terminal part of helix B and the outer loops of the β-subdomain. These interactions are part of the so called “latch”, that is believed to control the accessibility of the peptide binding site (1,6,13,16,30,31). The third mutant, DnaK3A, holds three substitutions (E531A/R536A/R547A) that hamper formation of two salt-bridges and a hydrogen bond between residues at helix B and helices C and D of the lid. The main difference between these proteins is that mutations in DnaK1A and DnaK2A modify the interaction between helix B and the β-sandwich subdomain, whereas those in DnaK3A might alter the interaction between helix B and the lid subdomain.

Multiple alignment of Hsp70 sequences reveals the conservation degree of residues mutated in this study (Fig. 1B). While D526/R445 is widely conserved among the Hsp70 family members, the ionic contacts at the latch are not equally conserved, and those within the lid show the lowest conservation degree.

Interaction with peptide substrates

The ability of wt and the three mutants to bind peptide substrates was analyzed by measuring the change in anisotropy of a fluorescence labeled peptide (F-APPY). In the presence of wt DnaK, the anisotropy value increases as the peptide binds DnaK, as previously reported (16,23,32). Equilibrium binding curves were obtained with increasing protein concentrations, and the anisotropy increase for each protein was fitted to a single site binding model (Fig. 2; Table 1). The mutants, particularly DnaK1A and DnaK3A, show a slightly decreased affinity for F-APPY (Table 1).

The kinetic parameters k_{+1} and k_{-1} were also estimated by following F-APPY binding at increasing protein concentrations. The data were fitted to a single exponential compatible with a single site binding model (Fig. 3A). From the linear plots of k_{obs} *vs.* protein concentration, k_{-1} (y-intercept) and k_{+1} (slope) were obtained (Fig. 3B). These parameters are clearly different for the mutants analyzed here, as seen in Table 1. While the kinetic constants of wt and DnaK3A are very similar, those of DnaK2A are 1.4-2 times higher, and the single mutation in DnaK1A induces a dramatic increase of the association (~160 fold) and dissociation (~27.4 fold) rates. The K_d values estimated from these kinetic parameters for wt DnaK, DnaK2A and DnaK3A also indicate that their affinity for F-APPY is comparable. In the case of DnaK1A, the binding process is too fast to obtain a reliable K_d value from kinetic measurements with our experimental time-resolution (see Fig. 3A), and only a rough estimation of the kinetic constants can be achieved. This behavior is similar to that observed for a DnaK lidless mutant (14,16).

As expected for a bimolecular reaction, increasing temperatures enhance the rate of DnaK-peptide complex formation, the final anisotropy value being slightly lower at higher temperatures (Figs. 4A and 4B). When the same experiment is performed with DnaK2A and DnaK3A, essentially the same temperature dependence of the peptide anisotropy is observed. It should be noted that the final protein concentration was adjusted (1 μM for wt DnaK, DnaK1A and DnaK2A; 3 μM for DnaK3A, Fig. 2A) to account for the differences in affinity, so that more than 90% of the added peptide substrate was bound. The stability of the substrate-protein complex against the thermal challenge is clearly different for DnaK1A mutant. In this case, the amount of bound peptide diminishes with temperature in such a way that at stress temperatures this mutant is unable to stably bind F-APPY (Figs. 4A and 4B). Cycling the sample between 25ºC and 42ºC induces reversible changes in the anisotropy of the DnaK1A-peptide mixture (Fig. 4C), indicating that the temperature-induced conformational transition responsible for the change in affinity of DnaK1A for F-APPY is reversible, as described for a lidless mutant of DnaK (16).

Secondary structure and stability of wt DnaK and the mutants.

The secondary structure of wt DnaK and the three mutants studied here was analyzed by CD spectroscopy. As shown in Fig. 5A, a comparison of the shapes and ellipticity values suggests that mutant proteins adopt a secondary structure similar to that of wt DnaK and therefore that mutations do not alter this structural level. To analyze whether the thermal stability of the protein was modified by the mutations, the ellipticity at 222 nm was measured as a function of temperature. Similar melting curves were obtained for wt DnaK, DnaK1A and DnaK2A mutants (Fig. 5B). They do display transitions with similar amplitudes at around 43ºC and 70ºC, as previously reported for the wild type protein (33). In contrast, the melting curve of DnaK3A displays a transition at around 45ºC while that at around 70ºC is hardly detected. It should be noted that the ellipticity value at 90ºC is similar for all proteins indicating that their thermally denatured conformation is also similar.

Protein stability was also characterized by DSC which provides the thermodynamic parameters of the unfolding process. The thermogram of wt DnaK (Fig. 6) shows three transitions that have been previously assigned (25). The lowest temperature transition comes from the unfolding of the ATPase domain, the second peak is due to the denaturation of the substrate binding domain, and the high temperature one contains contributions from the denaturation of both protein domains. The DSC profiles of all mutants differ considerably from that of wt DnaK. The thermogram of DnaK1A reflects a destabilization of the ATPase and substrate binding domains evidenced by a decrease of the temperature of the second transition (ΔT=6.5ºC), and by a 64% and 35% reduction in the enthalpy of their respective endotherms. Despite the drastic effect of this single amino acid replacement on the low temperature transitions, the third one remains essentially unchanged (Fig. 6; Table 2). To further prove that the low temperature endotherm in the DSC profile of DnaK1A was due to the denaturation of the ATPase domain, the same experiment was carried out in the presence of 1mM ADP. At this ligand concentration, only the T_m of the nucleotide binding domain of wt DnaK is upshifted by 9ºC (25), as it is observed for DnaK1A (data not shown), thus indicating that the above assignment also applies to this single point mutant.

Disruption of the ionic interactions at the latch in DnaK2A also modifies the thermal denaturation profile of the protein, although to a lesser extent. The only significant difference is a 27% decrease in the enthalpy of the second transition that is also downshifted ($\Delta T=2.5^{o}C$), while the temperature and calorimetric enthalpies of the other peaks are, as compared with DnaK1A, slightly affected (Fig. 6; Table 2). The thermal profile of DnaK3A shows that the temperatures of the first and second transitions are slightly shifted in opposite directions, their calorimetric enthalpy values being similar to those of the corresponding transitions of wt DnaK (Fig. 6; Table 2). However, the enthalpy of the third transition is reduced by 65% suggesting that, as found for a DnaK deletion mutant lacking helices C-E (16), denaturation of these helices that fold around a common hydrophobic core (6) gives rise to an endotherm at around 75ºC (Fig. 6; Table 2). The low enthalpy value is also in agreement with the weak intensity of the high temperature transition detected by CD for DnaK3A.

Nucleotide-induced conformational change: Partial proteolysis and fluorescence spectroscopy.

As previously reported for DnaK, partial proteolysis of the wt protein and the three mutants was used to gain information on their conformational properties, since the accessibility of the cleavage sites is related to the particular conformation that the protein adopts (17,20,34). Indeed, the pattern of tryptic fragments of DnaK is nucleotide-sensitive and has been used to differentiate the protein conformations corresponding to the high affinity (ADP-bound) and low affinity (ATP-bound) states for polypeptides (20). Since most of the cleavage sites are at the C-terminal domain, the different topology of the proteolytic sites is due to nucleotide-induced, allosteric conformational changes (Fig 7A). The tryptic patterns of all the proteins analyzed in this study showed only minor differences between the nucleotide-free (data not shown) and ADP-bound states, and therefore we will only compare trypsinolysis results obtained in the presence of ADP and ATP. As previously reported for wt DnaK (20), in the presence of ADP fragments with apparent molecular masses of 55, 46, 44, and 36 kDa were produced, and they were further digested to the 44 and 33-kDa truncated forms at longer incubation times. DnaK is degraded faster in the presence of ATP, and as compared with ADP the following differences could be noticed: i) a new 53 kDa fragment was obtained at short times, ii) the 46 kDa fragment was the most abundant at intermediate times, and iii) a 44 kDa fragment was finally produced as the major proteolytic species after 15 min incubation (Fig. 7A).

In contrast to wt DnaK, trypsin treatment processes almost all the ADP-state of DnaK1A at the shortest incubation time analyzed (1.5 min), generating major fragments of approx. 56 and 46 kDa that at longer times are converted into a 44 kDa one. Interestingly, this difference regarding the fragment pattern of the ADP-states of wt DnaK and DnaK1A is not observed for their ATP-states, the tryptic pattern being very similar for both proteins. Minor differences are seen for the 36 and 33 kDa fragments that regardless of the bound nucleotide are not detected with DnaK1A, instead two protein species of 18 and 16 kDa are observed.

A fragment similar to that of 56 kDa was attributed to tryptic cleavage around residue 500 of DnaK (20), therefore the appearance of the 56 kDa fragment at short incubation times of DnaK1A suggests that the C-terminal α-helices are more accessible to enzymatic cleavage in this mutant. This hypothesis has been confirmed by MS analysis of the 56 kDa major fragment, showing that it arises most likely from cleavage at amino acids K514 or R517 in helix A of the lid subdomain, since in contrast to wt DnaK that shows a good sequence coverage (83%) in the C-terminal α-helical subdomain, peptides beyond K514 are not found in the 56 kDa fragment (Fig. 7 B-C). The good agreement between the apparent molecular weight estimated from SDS-PAGE (56 kDa) and amino acid sequence (55.477 kDa and 55.896 kDa) for the 1-514 or 1-517 fragment, respectively, further supports this interpretation. The absence of fragments of 36 and 33 kDa in the pattern of nucleotide bound DnaK1A is likely due to further tryptic cleavage within its C-terminal region, as seen by MS analysis and in agreement with previous data (20). This sort of cleavage will also generate the low molecular weight fragments observed in DnaK1A.

The fragment patterns of both nucleotide-bound conformational states of DnaK2A are the same to those of wt DnaK. However DnaK3A, displays different tryptic sites. In the presence of ADP, DnaK3A generates a major fragment of approx. 62 kDa that at intermediate incubation times is also seen

together with a fragment of approx. 57 kDa and others already described for wt DnaK (see above; Fig. 7A). MS-MS analysis of the fragments detected only in DnaK3A (i.e., those with apparent molecular masses of 62 and 57 kDa, labeled in Fig. 7B as "b" and "c", respectively) are compatible with protein molecules comprising residues 1-577 or 1-581 and 1-527 which will have molecular masses of 62.204 or 62.733 and 56.906 kDa, respectively, in good agreement with the apparent values estimated from SDS-PAGE (Fig. 7 B-C). ATP induces a conformational change in DnaK3A evidenced by the disappearance of the 62 kDa fragment at short times and, as seen for wt DnaK, the appearance of the 53 kDa species. This might indicate that the ATP-induced conformational changes would protect the tryptic site that generates the 62 kDa fragment at the C-terminal helix bundle. Note that residue K581 is the ionic partner of residue E531 replaced by alanine in DnaK3A, and that residue K577 is located in its close vicinity.

Binding of ATP to DnaK quenches the fluorescence of its single Trp residue and shifts its emission maximum towards lower wavelengths (19,20). These spectroscopic changes require the interaction of both protein domains and therefore reflect allosteric communication. As already described for wt DnaK, ATP-binding to the three mutants induces a similar 4 nm blue-shift of their emission maxima and a 15% reduction of the fluorescence intensity (data not shown). These data suggest that the environment of W102 undergoes similar modifications in all proteins during the ATP-induced conformational changes.

Functionality of DnaK mutants.

To further assess the functional consequences of the structural differences presented so far, the effect of different ligands on the ATPase and refolding activities of wt DnaK and the three mutants was analyzed. The timing of the ATPase cycle has been proposed as an important factor that modulates the biological activity of DnaK and other Hsp70s (15), since it controls the transition between the substrate-accepting and releasing states of the protein, and is therefore regulated by co-chaperones and peptide substrates (17,29,35). The effect of NR peptide, GrpE and DnaJ on the ATPase activity of wild type and DnaK mutants is illustrated in Fig. 8A. Each of these ligands enhances the ATPase activity of all the proteins in a similar manner but when mixed together with the chaperone mimicking the physiological situation, DnaK1A is stimulated around 70 times in contrast to wt DnaK and the other two mutants whose ATPase activity is enhanced around 20-30 times.

Next, the effect of these mutations on the protein ability to refold chemically denatured luciferase was characterized (Fig. 8B). As previously published, wt DnaK was able to efficiently refold luciferase at 25 and 37ºC, whereas at 42ºC loses this ability (36). Essentially the same temperature-dependent refolding profile is observed for the DnaK3A mutant, indicating that loosening of the lid structure does not alter the refolding activity of the protein. In contrast, the chaperone activity of DnaK1A is temperature-dependent and while at 25ºC it refolds luciferase as wt DnaK, at 37ºC it cannot significantly refold this protein substrate. This is expected after analyzing the thermal stability of the substrate-DnaK1A complex that dissociates, at least partially, at 37ºC. This might not be the only reason why DnaK1A cannot properly refold protein substrates since DnaK2A, which stably binds peptide substrate, is unable to significantly reactivate this chemically denatured substrate regardless of the experimental temperature (Fig. 8B). A detailed study of this behavior is currently underway.

DISCUSSION

ATP binding to the DnaK ATPase domain generates an allosteric signal that is transmitted to both subdomains of the SBD (18). The allosteric conformational change most likely lowers the affinity of the β-subdomain for peptide substrates and modifies the position of the lid to allow peptide dissociation. The concerted allosteric structural rearrangement of both subdomains could be stabilized, particularly at stress temperatures, by a set of interactions between both subdomains and/or between any of these subdomains and the ATPase domain. Therefore, identification of the interactions involved in maintaining the location and/or dynamics of different protein regions is necessary to understand the functional cycle of DnaK. This is the goal of this work, where the contribution of ionic contacts at the interface of the two subdomains of the SBD, i. e., between residues at helix B and aminoacids at the lid or β-sandwich, to the conformational and functional properties of DnaK is analyzed.

Disruption of the highly conserved ionic pair D526-R445 has a strong effect in the conformation, stability and functional properties of the protein. Essential to describe this effect are the interactions that the N-terminus of αB establishes with the inner loop $L_{4,5}$. A detailed inspection of this protein region reveals that D526 interacts not only with R445 but also with K446, forming a "charged network" (Fig. 9). These types of charged networks have been found to stabilize protein structures (37). In the case of DnaK it might be important to fix the position of the C-terminal α-helices relative to the β-sandwich subdomain in the ADP-state of the protein. This assumption is corroborated by experimental evidence showing that disruption of these interactions control important structural and functional properties of DnaK. One piece of evidence is related to the enhanced trypsin accessibility of the interface between the C-terminal subdomains in the ADP-bound state of DnaK1A. A similar observation has been made for the apo-state of a Hsc70 mutant in which the counterion of D526, R447 was replaced by G (38). Our results also indicate that the conformational differences behind the higher susceptibility to proteolytic degradation might affect the lid structure and/or dynamics in the ADP-state of DnaK. If this were the case, the accessibility of the peptide binding site should be modified, as experimentally observed for both the association and dissociation constants of a peptide substrate, as previously described for DnaK(D526N) (39). This interpretation is further supported by a similar decrease in the thermal stability of the peptide-protein complexes observed for DnaK1A and a lidless mutant lacking helices B-E (16). This similarity also points to the possibility that other interactions between helix B and the β-sandwich might not be properly established if the ionic contacts in this protein region are disrupted.

Although DnaK1A possesses a significantly destabilized peptide binding site, faster substrate association and dissociation rates (Figs. 3 and 4), and higher stimulation of its ATPase activity by peptides and co-chaperones when added together (Fig. 8A), its folding activity is only compromised at 37ºC and not at 25ºC (Fig. 8B). It can therefore be assumed that the stability of the peptide-Hsp70 complex could control the chaperone function of the mutant and that co-chaperones do not stabilize the complex at physiological (37ºC) temperature. Under these experimental conditions, the substrate released from an unstable complex would join the irreversible aggregation process that kinetically competes with productive folding. It is interesting to note that the 3-fold higher cochaperone-mediated ATPase stimulation of DnaK1A also occurs at 37 ºC (data not shown), and that only at 25ºC the protein is able to refold denatured luciferase. It follows from this comparison that a normal refolding activity of this protein can coexist with an accelerated ATPase cycle, suggesting that both activities are not directly coupled.

The second effect of this mutation (D526A) is related to the reduction of the thermal stability of the β-sandwich subdomain and the ATPase domain of the protein, most likely due to modifications of interdomain interactions in which both subdomains of the SBD are involved (Figs. 5 and 6). Supporting this interpretation is the fact that a single substitution in DnaK1A destabilizes to a larger extent both domains of the apo-protein, as compared with the other two mutants. This finding might be a consequence of mutating a protein region that holds stabilizing interdomain interactions. In fact, both the NMR-derived model (12) and the X-ray structure (13) of two-domain truncated Hsp70 analogues propose the region formed by helix A and the N-terminus of helix B as an interdomain contact site in the absence of ligands. Indeed, αA and the N-terminus of αB are required to observe the ATP-induced fluorescence changes of W102 located at the subdomain IB of the DnaK ATPase domain (19). In summary, disruption of the ionic interaction in DnaK1A alters the conformation and/or dynamics of the lid in the ADP-state of the protein, and modifies interdomain interactions responsible for the stability of both protein domains. The involvement of this structural region in both interdomain interactions and contacts between the subdomains of the SBD might couple ATP binding to the NBD with lid displacement and peptide dissociation. Moreover, the interaction of J co-chaperones with this contact site (13,39) could be part of the structural mechanism by which J proteins regulate the functionality of both Hsp70 domains.

It is interesting to note that the conformational change brought about by this single amino acid replacement specially affects the ADP-bound state of the protein, i.e., the high-affinity conformation for substrates, while the ATP-state is similar to that of wt DnaK as

judged by partial proteolysis and fluorescence spectroscopy. This might reflect that this protein region could be part of the functional hinge that allows anchoring of both SBD subdomains in the ADP-state, and the displacement of the lid associated to the ATP-state of the protein. The functional cycle of DnaK has been analyzed assuming that in the ADP- and ATP-states the substrate binding site closes and opens, the rate of opening and closing being the main difference between both states (18). Two mechanisms have been proposed to explain the movement of the lid away from the peptide binding site that characterizes the open conformation. The first one is based on the two different lid conformations found in the X-ray structure of DnaK SBD (6). In one of them, the long helix B that folds over the binding site was kinked in the middle, suggesting that a hinge at this position of helix B allows the upwards movement of the lid. The second mechanism is supported by the different positions of the α-subdomain relative to the β-subdomain seen in two NMR analysis of truncated forms of Hsc70 and DnaK SBDs (4,5), and a crystal structure of truncated HscA SBD (11). Despite the limitations of the NMR structures that lack helices C-E and show a largely unfolded helix B that interacts with the peptide binding site, these structures suggest that the helical subdomain can occupy different positions with respect to the β-subdomain, and that opening of the peptide binding site could also be achieved by moving the entire helical subdomain. Our data support the view that the highly conserved interactions (see Fig. 1B) between the N-terminus of helix B and loop $L_{4,5}$ of the β-sandwich subdomain form part of the pivotal region that would function as a hinge to move the entire lid away from the binding site. Moreover, these interactions could be essential in defining the position of the lid in one of the two physiologically relevant conformations, the ADP-bound, high-affinity state for substrates, and therefore to define the lid movements during the functional cycle of the protein at 37ºC. If this were the case, movement of the entire α-helical subdomain might require modulation of other interactions, besides those mentioned above. Among these interactions are the ionic contacts between helix B and both subdomains of the SBD that are lost in DnaK2A and DnaK3A. Regarding mutations affecting to the latch in DnaK2A, it is interesting to note that they do not have as much impact in protein conformation (Fig. 7A), peptide association kinetics (Fig. 3; Table 1), thermal stability of the peptide-DnaK2A complex (Fig. 4), and in the stability of the protein structure (Figs. 5 and 6) as does the single mutation introduced in DnaK1A. However, the interactions forming the latch are critical in maintaining a functional DnaK cycle, since their disruption renders the protein unable to refold protein substrates under the experimental conditions used in this study. At present we cannot explain this behavior.

The three ionic interactions disrupted in DnaK3A have the expected effect on the compactness of the C-terminal α-helical structure, namely a lower thermal stability (Fig 6; Table 2) and an enhanced accessibility to tryptic cleavage (Fig 7). Interestingly, this accessibility is reduced in the presence of ATP indicating a conformational change in the C-terminal helix-bundle upon ATP binding, at least in mutant DnaK3A, that to our knowledge had not been previously detected in wild type DnaK. The modifications introduced in DnaK3A affect slightly the peptide binding properties of the protein (Figs. 2-4) but they do not alter the functionality of the mutant (Fig. 7), indicating that the compactness of the C-terminal helix-bundle is not essential for the DnaK refolding activity.

In summary, the results presented here demonstrate that the ionic contacts between the N-terminal region of helix B and the β-sandwich subdomain are necessary to stabilize the interaction between the lid and the β-subdomain in the ADP-bound state, that in turn controls the stability of the protein-substrate complex specially at high temperatures, and therefore the functional properties of DnaK. We propose that these interactions could be part of the functional hinge that regulates lid movements in Hsp70 proteins in response to ATP-binding.

REFERENCES

1. Mayer, M. P., and Bukau, B. (2005) *Cell. Mol. Life Sci.* **62**, 670-684
2. Flaherty K. M., Peluca-Flaherty, C. and McKay D. B. (1990) *Nature* **346**, 623-628
3. Morshauser, R.C., Wang, H., Flynn, G. C. and Zuiderwerg, E. R. (1995) *Biochemistry* **34**, 6261-6266.
4. Morshauser, R. C., Hu, W., Wang, H., Pang, Y., Flynn, G. C. and Zuiderweg, E. R. (1999) *J. Mol. Biol*. **289**, 1387-1403.
5. Wang, H., Kurochkin, A. V., Pan, Y., Hu, W., Flynn, G. C. and Zuiderwerg, E. R. (1998) *Biochemistry* **37**, 7929-7940.
6. Zhu, X., Zhao, X., Burkholder, W. F., Gragerov, A., Ogata, C. M., Gottesman, M. E., and Hendrickson, W. A. (1996) *Science* **272,** 1606–1614.
7. Harrison, C. J., Hayer-Hartl, M., Di Liberto, M., Hartl, F. and Kuriyan, J. (1997) *Science* **276**, 431-435.
8. Pellecchia, M., Montgomery, D. L., Stevens, S. Y., Vander Kooi, C. W., Feng, H. P., Gierasch, L. M. and Zuiderweg E. R. (2000) *Nat. Struct. Biol*. **7**, 298-303.
9. Stevens, S. Y., Caif, S., Pellecchia, M., and Zuiderweg, E. R. P. (2003) *Protein Sci.* **12**, 2588-2596.
10. Zhang, Y. and Zuiderweg, E. R. (2004) *Proc. Natl. Acad. Sci. USA*. **101**, 10272-10277.
11. Cupp-Vickery, J. R., Peterson, J. C., Ta, D. T. and Vickery, L. E. (2004) *J. Mol. Biol*. **342**, 1265-1278.
12. Revington, M., Zhang, Y., Grovern, N. B., Alexander, Y.-V., Kurochkin and Zuiderweg, E. R. P. (2005) *J. Mol. Biol*. **349**, 163-183.
13. Jiang, J., Prasad, K., Lafer, E. M. and Sousa, R. (2005) *Mol. Cell*. **20**, 513-524.
14. Buckzynski, G., Slepenkov, V., Shorn, M. G. and Witt, S. N. (2001) *J. Biol. Chem*. **276**, 27231-27236.
15. Slepenkov S. V. and Witt, S. N. (2002) *Biochemistry* **41**, 12224-12235.
16. Moro, F., Fernández-Sáiz, V. and Muga, A. (2004) *J. Biol. Chem*. **279**, 19600-19606.
17. Liberek, K., Skowyra, D., Zylicz, M., Johnson, C. and Georgopoulos, C. (1991) *J. Biol. Chem*. **266**, 14491−14496.
18. Mayer, M. P., Laufen, T., Paal, K., McCarty, J. S. and Bukau, B. (2000) *Nat. Struct. Biol*. **7**, 586-593.
19. Moro, F., Fernández, V. and Muga, A. (2003) *FEBS Lett.* **533**, 119.123.
20. Buchberger, A., Theyssen, H., Schröder, H., McCarty, J. S., Virgallita, G., Milkereit, P., Reinstein, J. and Bukau, B. (1995) *J. Biol. Chem*. **270**, 16903−16910.
21. Zylicz, M., Yamamoto, T., Mc Kittrick, N., Sell, S and Geosgopoulos C. (1985) *J. Biol. Chem*. **260**, 7591-7598.
22. Mehl, A. F., Heskett, L. D. and Neal. K. M. (2001) *BBA.* **282**, 562-569.
23. Montgomery, D.L., Morimoto R. I. and Gierasch, L. M. (1999) *J. Mol. Biol.* **296**, 915-932.
24. Moro, F, Fernandez-Saiz, V., Slutsky, O., Azem, A., and Muga, A. (2005) *FEBS J*. 272, 3184-3196.
25. Montgomery, D., Jordan, R., McMacken, R. and Freire, E. (1993) *J. Mol. Biol.* **232**, 680-692.
26. Shevchenko, A., Loboda, A., Shevchenko, A., Ens, W. and Standing, K. G. (1996) *Anl. Chem.*. **68**, 850-858.
27. Gobom, J., Nordhoff, E., Mirgorodoskaya, E., Ekman, R. and Roepstorff, P. (1999) *J. Mass Spect*. **34**, 105-116.
28. Larsen, M. R., Cordwell, S.J. and Roepstorff, P. (2002) *Proteomics* **9**, 1277-1287.
29. Pierpaoli, E. V., Sandmeier, E., Schonfeld, H. J. and Christen, P. (1998) *J. Biol. Chem*. **273** 6643-6649.
30. Ha, J.-H., Hellman, U., Jonson, E. R., Li, ., McKay, D. B. Sousa, M. C., Takeda, S., Wernstedt, C. and Wilbanks, S. M. (1997) *J. Biol. Chem*. **272**, 27796-27803.
31. Chang, T.-C., Hsiao, C.-D., Wu, S.-J. and Wang, C. (2001) *Arch. Biochem. Biophys*. **386**, 30-36.
32. Davis, J. E., Voisine, C. and Craig, E. A. (1999) *Proc. Natl. Acad. Sci. USA*. **96**, 9269-9276.

33. Palleros, R. D., Shi, L., Reid, L. Katherine and Fink, L. A. (1994) *J. Biol. Chem*. **269**, 13107-13144.
34. Kamath-Loeb, A. S., Lu, C. S., Suh, W. C., Loneto, M. A. and Gross, C. A. (1995) *J. Biol. Chem*. **270**, 30051−30059.
35. Jordan, R. and McMacken, R. (1995) *J. Biol. Chem*. **270**, 4583-4569.
36. Brehmer, D., Gässler, C., Rist, W., Mayer, P. M. and Bukau, B. (2004) *J. Biol. Chem*. **279**, 27957−27964.
37. Horovitz, A., Serrano, L., Avron, B., Bycroft, M. and Fersht, A. R. (1990) *J. Mol Biol.* **216**, 1031-1044.
38. Hu, S.-M., Liang, P.-H., Hsiao, C.-D. and Wang, C. (2002) *Arch. Biochem. Biophys*. **407**, 135-141.
39. Suh, W. C., Burkholder, W. F., Lu, C. Z., Zhao, X., Gottesman, M. E., and Gross, C. A. (1998) *Proc. Natl. Acad. Sci. U S A*. **95**, 15223-8.
40. Vriend, G. (1990) *J. Mol. Graph*. **8**, 52-56.

FOOTNOTES

V. F.-S. and S. P.-A. are recipients of predoctoral fellowships from the Basque Government, and F. M. holds an I3P contract (CSIC). We thank S. Taneva and F. M. Goñi for critically reading the manuscript. F. Elorza (CIC bioGUNE) and K. Aloria (Sgiker, UPV) are gratefully acknowledged for MS analysis. This work was supported by MEC (BFU 2004-03452/BMC) and the University of the Basque Country (UPV 13505/2001).

[1]The abbreviations used are: DnaK1A, DnaK(D526A); DnaK2A, DnaK(D540A/K548A); DnaK3A, DnaK(E531A/R536A/R547A); DSC, differential scanning calorimetry; CD, circular dichroism; MS, mass spectrometry; MALDI, matrix-assisted laser desorption ionization; ESI, electrospray ionization; NBD, nucleotide binding domain; SBD, substrate binding domain.

FIGURE LEGENDS

Fig. 1. An outline of the mutants used in this study. *A,* Ribbon diagram of part of the substrate binding domain of DnaK (PDB:1DKX). Residues replaced in mutant DnaK1A, DnaK2A, and DnaK3A, are shown in green, blue and red color, respectively. All these residues are located in the long helix B that is colored in yellow. The corresponding ionic partners, the bound peptide, the loops protruding from the β-sandwich subdomain ($L_{4,5}$, $L_{1,2}$, $L_{3,4}$, $L_{5,6}$) and the α-helical segments (αA-E) are indicated. *B,* Multiple sequence alignment (ClustalW) of the SBD of DnaK, bovine -Hsp70b-, human-Hsp70h-, yeast endoplasmic reticulum –BIP- and mitochondrial -Ssc1p- Hsp70s. Fully conserved amino acids are indicated with *asterisk*, and positions mutated in DnaK1A, DnaK2A and DnaK3A are shown in green, blue and red, respectively. Replaced residues in helix B of the mutants are depicted in the upper box and their corresponding partners in the lower boxes. Residues are numbered following the DnaK sequence.

Fig. 2. Equilibrium binding curves of F-APPY peptide to wt DnaK and mutants. Fluorescence anisotropy was determined at 35 nM peptide and increasing Hsp70 concentrations. Wt DnaK, filled circle; DnaK1A, filled triangle; DnaK2A, open square; DnaK3A, open diamond. Solid lines are the best fit of the data to a single site binding model as indicated in the text.

Fig. 3. Kinetics of F-APPY interaction with wt DnaK and mutant Hsp70s. *A,* Titration with increasing Hsp70 concentrations. DnaK and Hsp70s mutants were injected into a 35 nM F-APPY sample at 25ºC. Representative kinetics of DnaK (filled circles; 0.5, 1 and 2 μM) and DnaK1A (grey circles; 0.05, 0.1, 0.2 and 0.4 μM) interaction with the peptide substrate. All kinetics were accurately fitted with the single exponential function $y = y_0 + a(1-e^{-kx})$ (solid lines). *B,* Estimation of the kinetic constants for the Hsp70-peptide interaction. k_{-1} and k_{+1} are derived from the y-intercept and the slope, respectively. Wt DnaK, filled circle; DnaK1A, filled triangle; DnaK2A, open square; DnaK3A, open diamond.

Fig. 4. Thermal stability of the Hsp70-peptide complexes. *A*, F-APPY binding kinetics of DnaK, DnaK1A, DnaK2A and DnaK3A, measured at 25, 37 and 42ºC. Binding was analyzed in the presence of 0.5 mM ADP to stabilize the ATPase domain of the proteins (25), and initiated by addition of F-APPY (35 nM final concentration) to a thermostated solution of Hsp70 protein (1 μM wt DnaK, DnaK1A and DnaK2A, and 3 μM DnaK3A). *B*, Anisotropy increment at the saturation plateau for DnaK, DnaK1A, DnaK2A and DnaK3A at 25, 37 and 42ºC. Values were obtained after fitting the experimental data to single exponential curves. *C*, Temperature-induced inhibition of substrate binding to DnaK1A is reversible. 1 μM DnaK1A and 35 nM F-APPY were incubated at 25ºC to achieve maximum binding, then the temperature was raised to 42ºC and lowered again to 25ºC while continuously measuring the anisotropy value.

Fig. 5. Secondary structure of wt DnaK and mutants. *A*, Far UV-CD spectra of wt DnaK and mutants in 20 mM borate, pH 9.0 buffer. Wt DnaK, solid line; DnaK1A, dotted-line; DnaK2A, dashed-line; DnaK3A, dotted-dashed-line. *B*, Thermal stability of the same samples followed by the change in ellipticity at 222 nm as a function of temperature. Wt DnaK, solid line; DnaK1A, dotted-line; DnaK2A, dashed-line; DnaK3A, dotted-dashed-line.

Fig. 6. Thermal stability of wt DnaK and constructed mutants. DSC traces of wt DnaK, DnaK1A, DnaK2A and DnaK3A. Experiments were carried out in 25 mM glycine, pH 9.0, at 1-2 $mg \cdot ml^{-1}$ protein concentration. Scan rate was 60ºC/h. Circles represent the experimental points, dashed lines the result of the best fit obtained from deconvolution analysis assuming a three-transition model, and solid lines the overall fit.

Fig. 7. Partial proteolysis of wt DnaK and its mutants. Mutants DnaK1A and DnaK3A, but not DnaK2A, show an altered nucleotide-induced C-terminal conformation. *A*, Aliquots of a partial tryptic digestion of DnaK and mutants in the presence of 1 mM ADP (middle panel) or ATP (right-hand panel) were taken at the indicated incubation times and analyzed in 12.5 %. SDS-PAGE. The left-hand panel corresponds to time 0. The left-hand lane in each panel contains molecular weight markers. *Asterisk* indicates the trypsin band. *B*, ADP-tryptic fragments selected for MS analysis. The molecular weights estimated from SDS-PAGE (calculated using the plot $\log_{MW}$ *vs*. R_f and corrected to obtain a MW of 69.037 for wt DnaK) and from MS are compared. *C*, Identification of additional tryptic cleavage sites in the ADP-state of DnaK1A and DnaK3A. Last amino acid residues detected in the proteolytic fragments labeled as "a", "b" and "c" are highlighted in bold in the amino acid sequence of the mutants. Localization of the cleavage sites is indicated in the secondary structure outline. *Asterisks* indicate the Ala residues replacing wt residues in the mutants.

Fig. 8. Functionality of DnaK and mutants. *A*, Stimulation of the ATPase activity by peptide and co-chaperones. Steady-state ATPase activity was measured at 30ºC at a protein and ATP concentrations of 3 μM and 1 mM, respectively. NR (NRLLLTG) peptide, DnaJ and GrpE were added at 300 μM, 0.3 μM and 0.9 μM, respectively. *B*, Luciferase refolding activity. Reactivation of GndHCl-denatured luciferase by wt DnaK and mutants DnaK1A, DnaK2A and DnaK3A at 25, 37 and 42ºC was achieved as described in *Experimental Procedures.* Control refers to refolding in the absence of chaperones.

Fig. 9. Network of ionic interactions in which D526A is involved (PDB:1DKX). D526 at the N-terminal region of helix B establishes two ionic contacts with residues R445 and K446 at the inner loop $L_{4,5}$. This triad may also stabilize other contacts between the β-sandwich and helices A and B, as indicated. The atomic distances, measured by WHAT IF software (40), between selected charged amino acid residues are given in Å.

Table 1. F-APPY dissociation and binding constants. k_{+1} and k_{-1} were obtained at 25ºC. K_d values were determined under equilibrium conditions (see Experimental Procedures).

	K_d μM	k_{+1} ($M^{-1} \cdot s^{-1}$)	k_{-1}($s^{-1} \cdot 10^3$)
DnaK	0.11 (± 0.009)	570	0.60
DnaK1A	0.25 (± 0.019)	91400*	16.45*
DnaK2A	0.18 (± 0.013)	1376	0.81
DnaK3A	0.41 (± 0.007)	614	0.50

* These values are a rough estimation of the kinetic constants (see text).

Table 2: Thermodynamic parameters associated to the thermal denaturation of DnaK and the alanine exchanged mutants.

	Transition 1		Transition 2		Transition 3	
	T_m (ºC)	ΔH_{cal} (kcal/mol)	T_m (ºC)	ΔH_{cal} (Kcal/mol)	T_m (ºC)	ΔH_{cal} (kcal/mol)
wt DnaK	43.5	79	57.5	94	74	72
DnaK1A	45.7	28.1	51	61	73.6	75
DnaK2A	43.9	66	55	68	75.6	57
DnaK3A	46.2	90	54	98	76.5	24

T_m is the temperature at which the maximum excess heat capacity occurs, and ΔH_{cal} is the calorimetric transition enthalpy. Values are the average of at least two independent experiments on two different protein batches. The experimental error is lower than ± 0.4ºC for T_m and 15% for ΔH_{cal}.

FIGURE 1

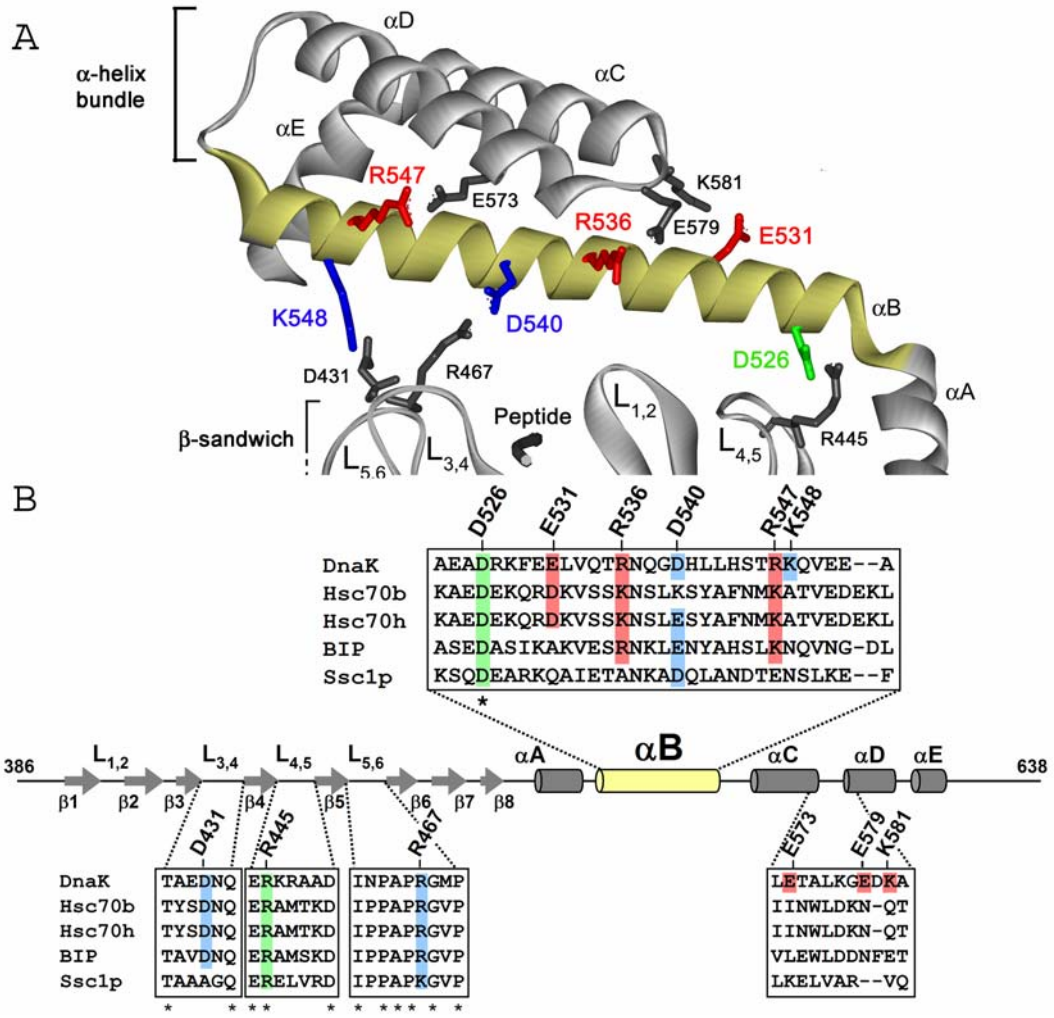
A
α-helix bundle
αD
αC
αE
R547
E573
K581
R536
E579
E531
K548
D540
αB
D526
D431
R467
β-sandwich
Peptide
L1,2
L4,5
R445
αA
L5,6
L3,4
B
D526
E531
R536
D540
R547
K548
DnaK AEADRKFEELVQTRNQGDHLLHSTRKQVEE--A
Hsc70b KAEDEKQRDKVSSKNSLKSYAFNMKATVEDEKL
Hsc70h KAEDEKQRDKVSSKNSLESYAFNMKATVEDEKL
BIP ASEDASIKAKVESRNKLENYAHSLKNQVNG-DL
Ssc1p KSQDEARKQAIETANKADQLANDTENSLKE--F
386
L1,2
L3,4
L4,5
L5,6
αA
αB
αC
αD
αE
638
β1
β2
β3
β4
β5
β6
β7
β8
D431
R445
R467
E573
E579
K581
DnaK TAEDNQ ERKRAAD INPAPRGMP LETALKGEDKA
Hsc70b TYSDNQ ERAMTKD IPPAPRGVP IINWLDKN-QT
Hsc70h TYSDNQ ERAMTKD IPPAPRGVP IINWLDKN-QT
BIP TAVDNQ ERAMSKD IPPAPRGVP VLEWLDDNFET
Ssc1p TAAAGQ ERELVRD IPPAPKGVP LKELVAR--VQ

FIGURE 2

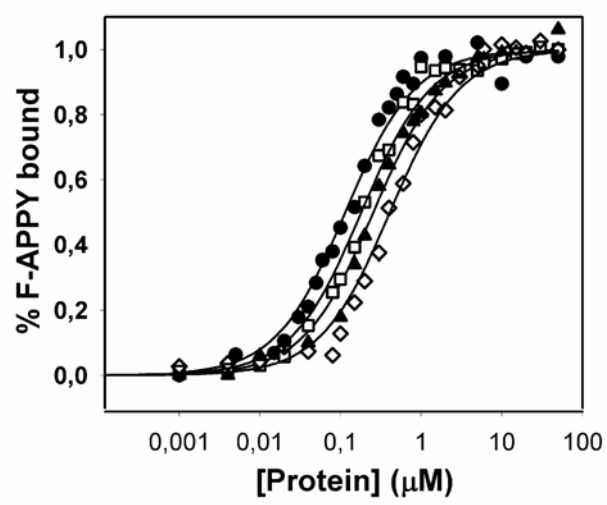

FIGURE 3

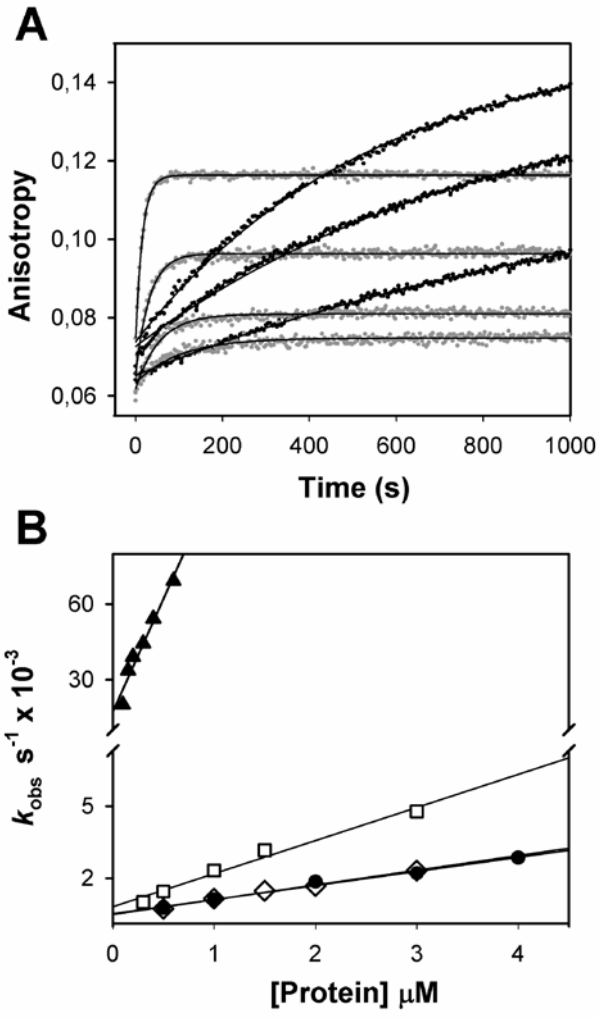
A
Anisotropy
0,14
0,12
0,10
0,08
0,06
0
200
400
600
800
1000
Time (s)
B
k_{obs} s^{-1} x 10^{-3}
60
30
5
2
0
1
2
3
4
[Protein] μM

FIGURE 4

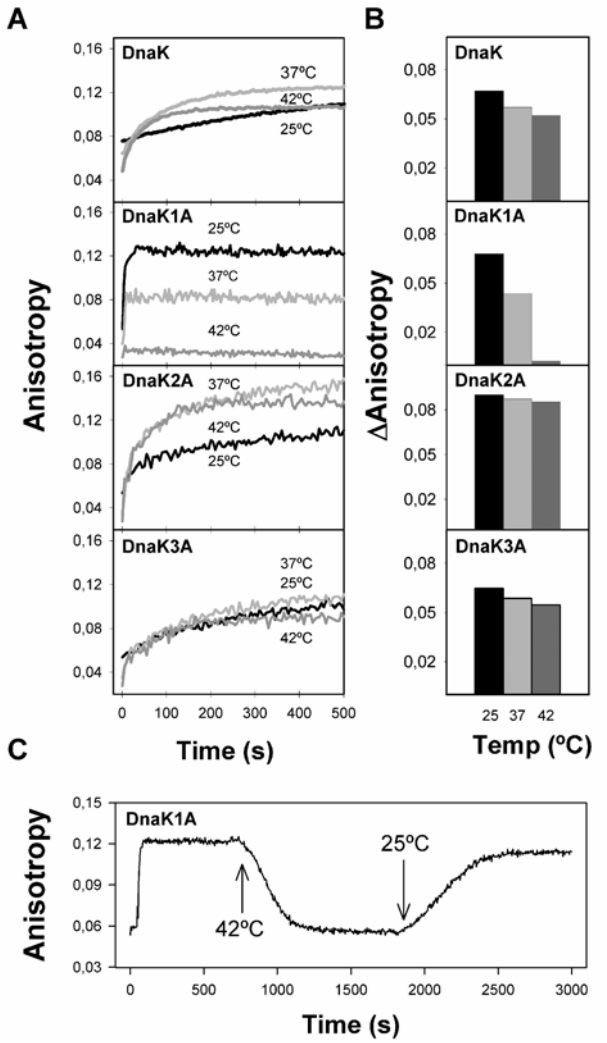
A
B
C
DnaK
DnaK1A
DnaK2A
DnaK3A
37ºC
42ºC
25ºC
Anisotropy
ΔAnisotropy
Time (s)
Temp (ºC)
0,16
0,12
0,08
0,04
0,05
0,02
0 100 200 300 400 500
25 37 42
0,15
0,09
0,06
0,03
0 500 1000 1500 2000 2500 3000

FIGURE 5

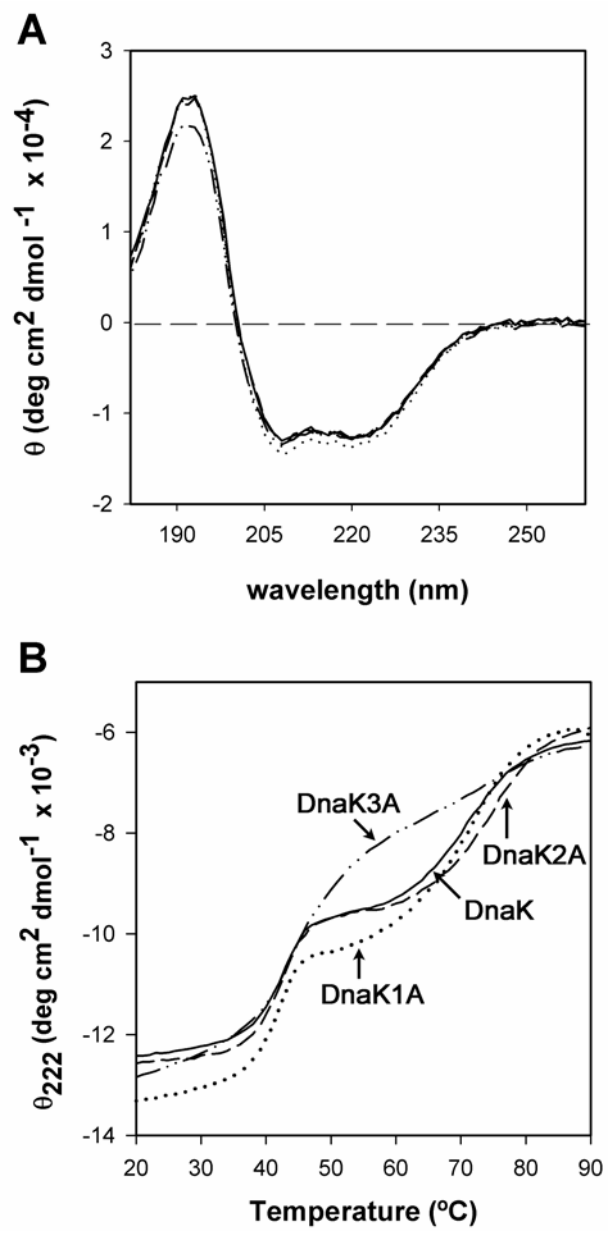
A
θ (deg cm2 dmol -1 x 10-4)
3
2
1
0
-1
-2
190
205
220
235
250
wavelength (nm)
B
θ222 (deg cm2 dmol-1 x 10-3)
-6
-8
-10
-12
-14
20
30
40
50
60
70
80
90
Temperature (ºC)
DnaK3A
DnaK2A
DnaK
DnaK1A

FIGURE 6

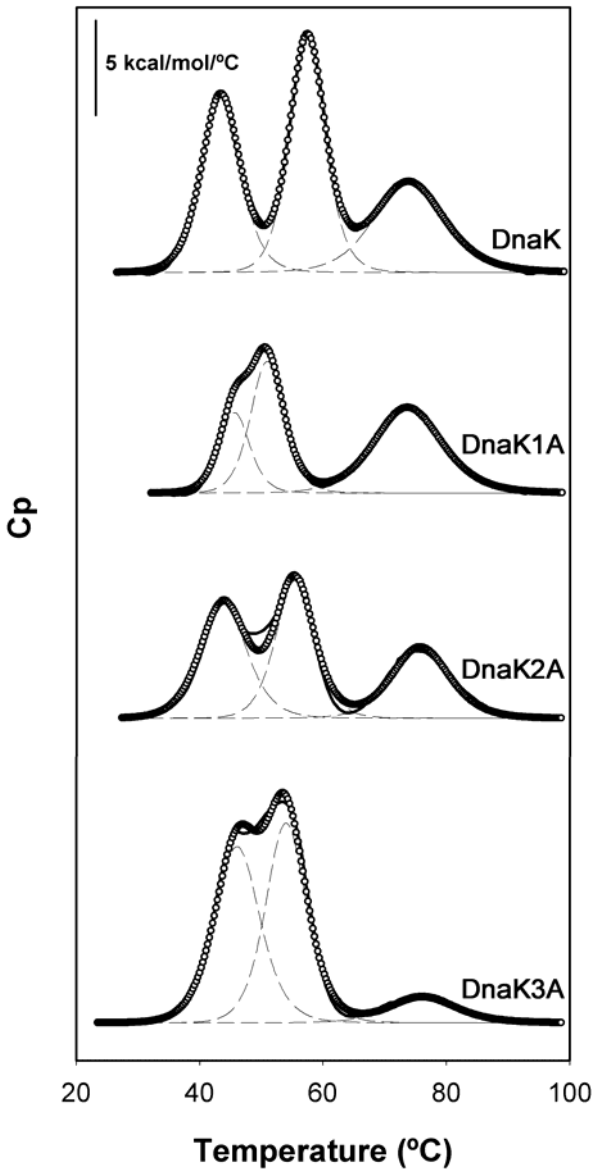
5 kcal/mol/ºC
DnaK
DnaK1A
DnaK2A
DnaK3A
Cp
20
40
60
80
100
Temperature (ºC)

FIGURE 7

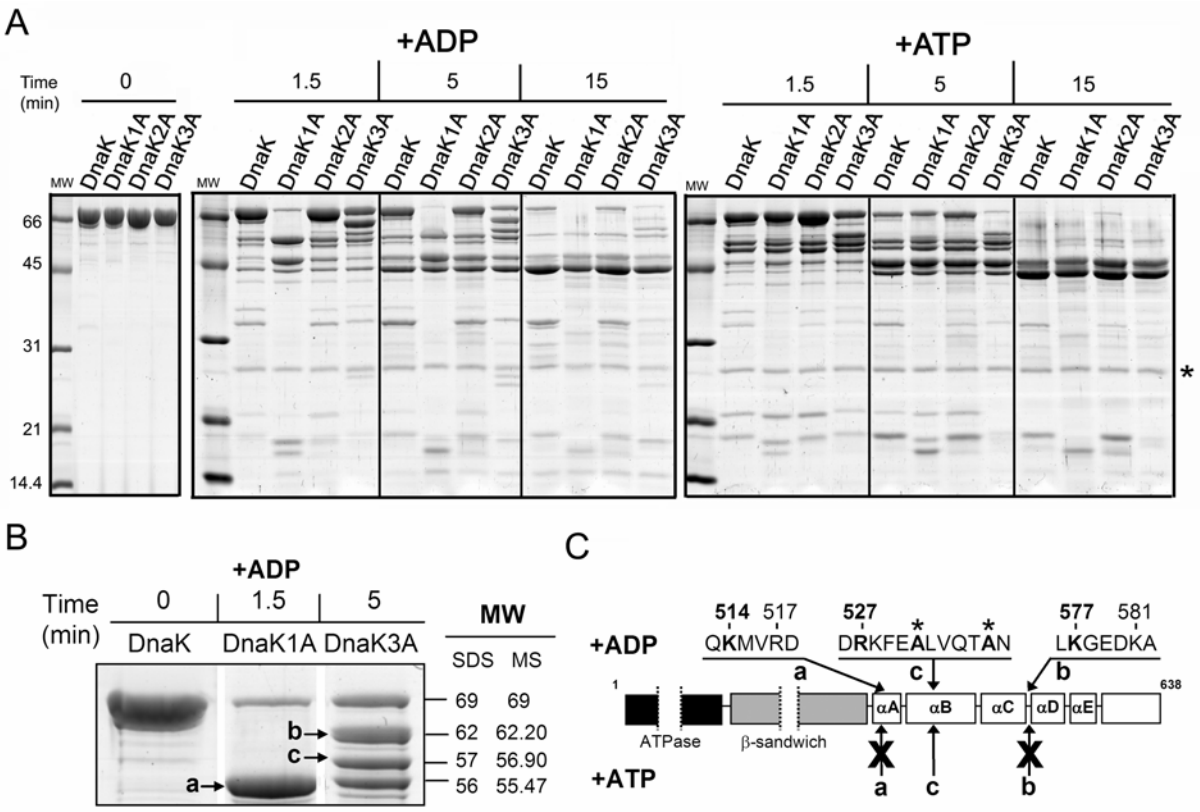
A
+ADP
+ATP
Time (min)
0
1.5
5
15
MW
DnaK
DnaK1A
DnaK2A
DnaK3A
66
45
31
21
14.4
*
B
+ADP
Time (min)
0
1.5
5
DnaK
DnaK1A
DnaK3A
MW
SDS
MS
69
69
62
62.20
57
56.90
56
55.47
a
b
c
C
+ADP
+ATP
514 517
QKMVRD
527
DRKFEALVQTAN
577 581
LKGEDKA
1
638
ATPase
β-sandwich
αA
αB
αC
αD
αE
a
c
b

FIGURE 8

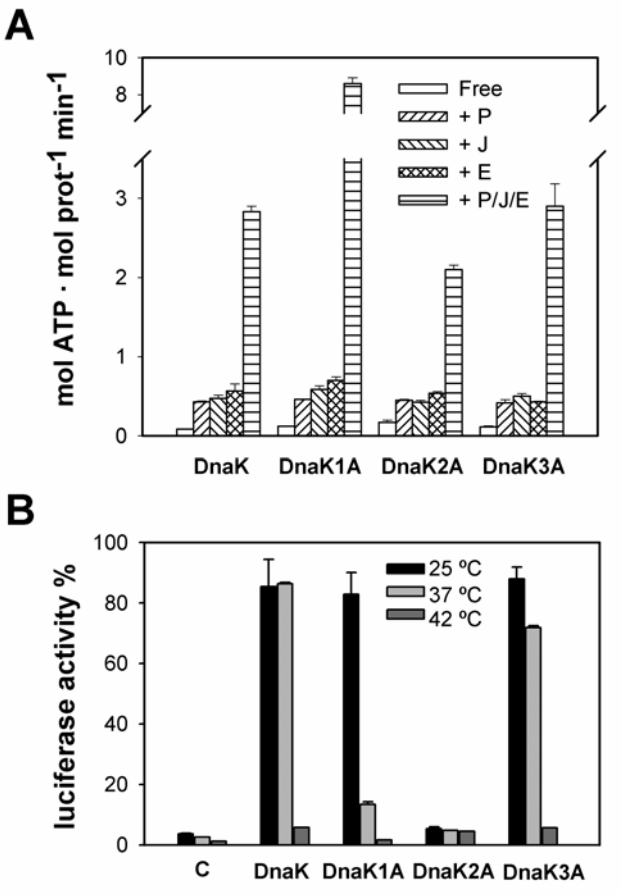
A
mol ATP · mol prot-1 min-1
10
8
3
2
1
0
Free
+ P
+ J
+ E
+ P/J/E
DnaK
DnaK1A
DnaK2A
DnaK3A
B
luciferase activity %
100
80
60
40
20
0
25 ºC
37 ºC
42 ºC
C
DnaK
DnaK1A
DnaK2A
DnaK3A

FIGURE 9

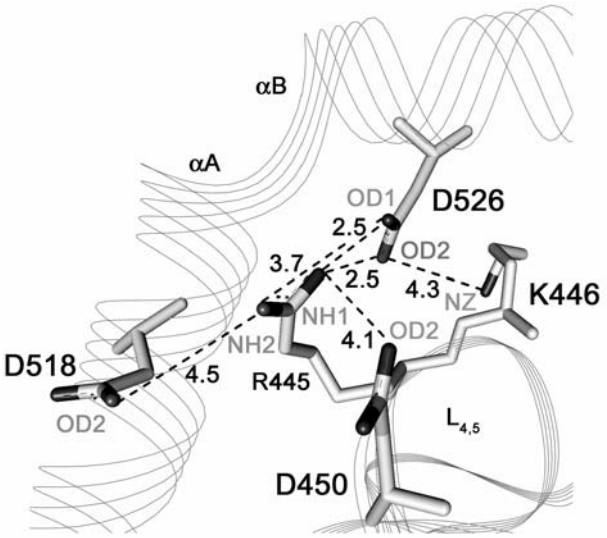
αB
αA
OD1
D526
2.5
OD2
3.7
2.5
4.3
NZ
K446
NH1
OD2
4.1
NH2
D518
4.5
R445
OD2
L4,5
D450